

Angle-dependent planar thermal Hall effect by quasi-ballistic phonons in black phosphorus

Xiaokang Li,^{1,*} Xiaodong Guo,^{1,2} Zengwei Zhu,^{1,†} and Kamran Behnia^{2,‡}

¹Wuhan National High Magnetic Field Center, School of Physics, Huazhong University of Science and Technology, Wuhan 430074, China

²Laboratoire de Physique et d'Etude de Matériaux (CNRS) ESPCI Paris, PSL Research University, 75005 Paris, France

The origin of the phonon thermal Hall effect in insulators is a matter of ongoing debate. The large amplitude of the signal in an elemental non-magnetic solid, such as black phosphorus (BP) calls for a minimal mechanism with no role for spin degree of freedom. Here, we show that a longitudinal heat flow generates a transverse temperature gradient in BP even when the magnetic field, the heat current and the thermal gradient lie in the same plane. The long phonon mean-free-path leaves little room for scattering by point-like symmetry breaking defects. We show that the signal peaks when the magnetic field is oriented along one of the two diagonal orientations of the puckered honeycomb plane and argue that this can be understood as the sum of two distinct contributions each parallel to a mirror plane. This angular dependence as well as the order of magnitude of the observed signal points to the torque exerted by magnetic field on electric dipoles traveling with heat-carrying phonons as the driver of the effect.

The thermal conductivity is a second rank tensor linking the heat current density and the temperature gradient vectors. The thermal Hall effect (THE) refers to non-zero off-diagonal components of this tensor, $\bar{\kappa}$. Its phonon-driven origin in insulators has attracted much recent experimental [1–17] and theoretical [18–26] interest. More recently, attention has focused on the observation of a planar thermal Hall effect [15–17]. This is a configuration with the three relevant vectors (Heat current, temperature gradient and magnetic field) lying in the same plane. The persistence of the signal when the signal is forbidden by crystal symmetry was attributed to defects breaking the local symmetry [17].

Here, we report on the observation of a planar Hall effect in black phosphorus (P), an elemental insulator with ballistic phonons [27] and no magnetism. The thermal conductivity tensor has unequal diagonal components ($\kappa_{zz} \simeq 5\kappa_{xx}$). Nevertheless, the off-diagonal components match each other ($\kappa_{xz}(B) \simeq \kappa_{zx}(-B)$), as expected by Onsager reciprocity. We quantify the variation of the thermal Hall signal as a function of the in-plane orientation of the magnetic field and find that it displays a twofold oscillation with minimum and maximum along one of the two diagonals of the xz plane of the puckered honeycomb lattice. This indicates that the signal is the sum of two sinusoidal contributions along two high-symmetry axes. A quantitative account of our observation is missing. Nevertheless, we argue that a scenario in which electric dipole moments, generated by the thermal gradient and the atomic vibrations, play a key role is compatible with the order of magnitude of the observed signal as well as its angular variation.

Fig. 1a shows the crystal structure of black P. Identical phosphorus atoms located on two distinct sites are marked in blue and red. Each layer is a puckered honeycomb lattice in the xz crystallographic plane, where the

x and z axes correspond to the armchair and zigzag orientations. As seen in Fig. 1b, the longitudinal thermal conductivity, as found previously [27, 28], is significantly different along the two orientations. Along the zigzag orientation, thermal conductivity is much larger than along the armchair orientation in the low temperature limit. The sound velocity shows a similar but attenuated anisotropy (9.6 km/s along z -axis *vs.* 4.6 km/s along the x -axis) [29]. As a consequence, the phonon mean free path $\ell_{ph}(T)$, shown in Fig. 1c, is also anisotropic. It is twice longer along the z -axis and approaches the sample thickness (30 μm) around 20 K. Thus, at this temperature phonons become quasi-ballistic and accordingly thermal conductivity becomes size dependent [27].

A Hall response refers to a signal odd in magnetic field and oriented perpendicular to the applied current. Designating the transverse temperature gradient by $(\nabla T)_\perp$, the applied longitudinal heat current by J_q and the magnetic field by B , the standard thermal Hall configuration corresponds to $B \perp J_q \perp (\nabla T)_\perp$. It is sketched in panel d and was the subject of our previous study [12]. Panel e shows the configuration for planar thermal Hall effect, which corresponds to $B \parallel (J_q \perp (\nabla T)_\perp)$. We use κ_{ij}^k to designate the $\bar{\kappa}$ component corresponding to J_q along the i -axis, $(\nabla T)_\perp$ along the j -axis and the magnetic field along the k -axis.

Fig. 2a-c shows the planar thermal Hall data for three different configurations. In each panel, the orientations of the three relevant vectors (B , J_q and $(\nabla T)_\perp$) are sketched and the field dependence of the ratio of the transverse to longitudinal temperature gradients ($\nabla T_j / \nabla T_i$) is shown.

Fig. 2d compares the temperature dependence of the thermal Hall angle in three planar configurations at 12 T. It is finite in the three planar configurations, but there is a large difference in amplitude when one permutes the orientations of J_q and $(\nabla T)_\perp$. Since the longitudinal

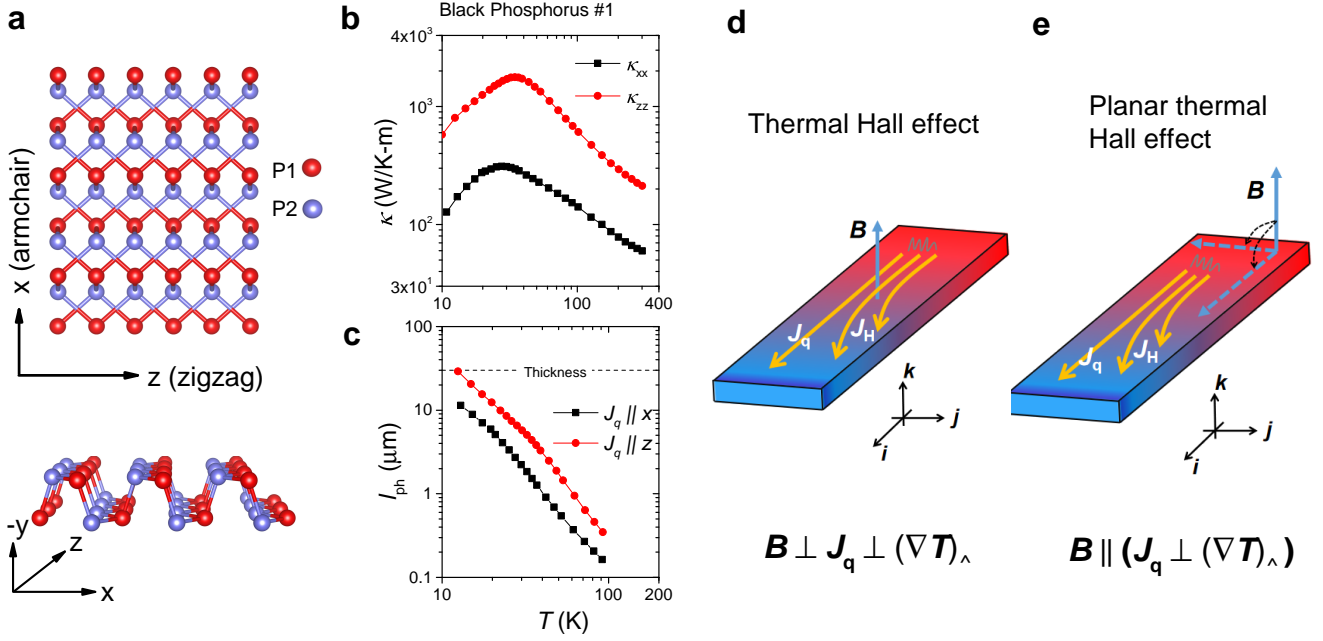


FIG. 1. **Crystal structure, phonon mean free path and two versions of the thermal Hall effect.**(a) Top (two layers) and side (single layer) view of the lattice of black phosphorus (BP). P atoms, marked in blue and red, belong to atomic sites with distinct environments. The x and z axes respectively correspond to the armchair and zigzag directions of the BP layer plane. (b) Longitudinal thermal conductivity (from previous work [12]) along the armchair (κ_{xx}) and the zigzag (κ_{zz}) orientation, at least four times of anisotropy can be seen. (c) The temperature dependence of mean free path of phonon (l_{ph}) in BP for two in-plane orientations ($J_q \parallel z$ axis and $J_q \parallel x$ axis), extracted from the longitudinal thermal conductivity, the sound velocity and the specific heat. It shows an increasing behavior before 10 K with cooling and is comparable to the sample thickness around 20 K, the peak temperature of κ_{ii} . (d) The schematic for measuring the thermal Hall effect, with the magnetic field (B) perpendicular to the longitudinal heat current (J_q) and the transverse thermal gradient ($(\nabla T)_\perp$). The thermal Hall conductivity tensor is denoted as κ_{ij}^k . (e) The schematic for measuring planar thermal Hall effect, with the magnetic field (B) rotating from the orthogonal to the parallel direction of the J_q or the $(\nabla T)_\perp$. Two types of planar thermal Hall conductivity tensors are denoted as κ_{ij}^i and κ_{ij}^j respectively.

thermal conductivity is anisotropic by the same factor, this difference warrants an equality between the absolute values of κ_{xz}^z and κ_{zx}^z , as expected by Onsager reciprocity.

The thermal Hall angle (Fig. 2d) combined with the longitudinal thermal conductivity (Fig. 1b) leads to the planar thermal Hall conductivity, which is shown in Fig. 2e and f. The thermal Hall response is finite in four distinct configurations. We can see not only the validity of the Onsager reciprocity (Fig. 2e), but also the very small influence of the orientation of magnetic field on the amplitude of κ_{xz} (Fig. 2f).

We then proceeded to quantify the angle dependence of this planar Hall signal at fixed temperature as the magnetic field rotated in the xz plane. The raw data, shown in the supplement [30], shows a field-linear response for all explored angles. The measurements were performed at 44.5 K. This temperature was chosen to allow a compromise between proximity to the peak temperature and the optimal sensitivity of the thermocouples. As seen in Fig. 3a, the signal shows a twofold oscillation. It peaks (with opposite signs) at $\phi = -\pi/4$ and $\phi = 3\pi/4$ i.e.

along one of the diagonals of the xz plane, and vanishes along the other diagonal. This intriguing feature would find a straightforward interpretation if the signal is the sum of two contributions of equal amplitude shifted by $\pi/2$, one following $\cos\phi$ (peaking along the x -axis and vanishing along the z -axis) and another following $\cos(\phi + \pi/2)$ (peaking along the z -axis and vanishing along the x -axis), indicated by dashed lines in Fig. 3a. As sketched in Fig. 3b, each odd-field contribution would be bounded to one mirror plane.

Thus, we detect in a crystal belonging with the mmm point group symmetry, there is a planar thermal Hall signal with bi-axial symmetry. Let us note that at peak temperature of this thermal Hall signal, the longitudinal thermal conductivity of black P is as large as $\kappa_p \simeq 2000$ W/Km. This is to be compared with cases such as α -RuCl₃ ($\kappa_p \simeq 3$ W/Km) [11], Na₂Co₂TeO₆ ($\kappa_p \simeq 10$ W/Km) [16] or Y-kapellasite ($\kappa_p \simeq 2$ W/Km) [17]. Contrary to these cases, the phonon mean free path in black P is close to the sample dimensions and local defects are unlikely to play a major role.

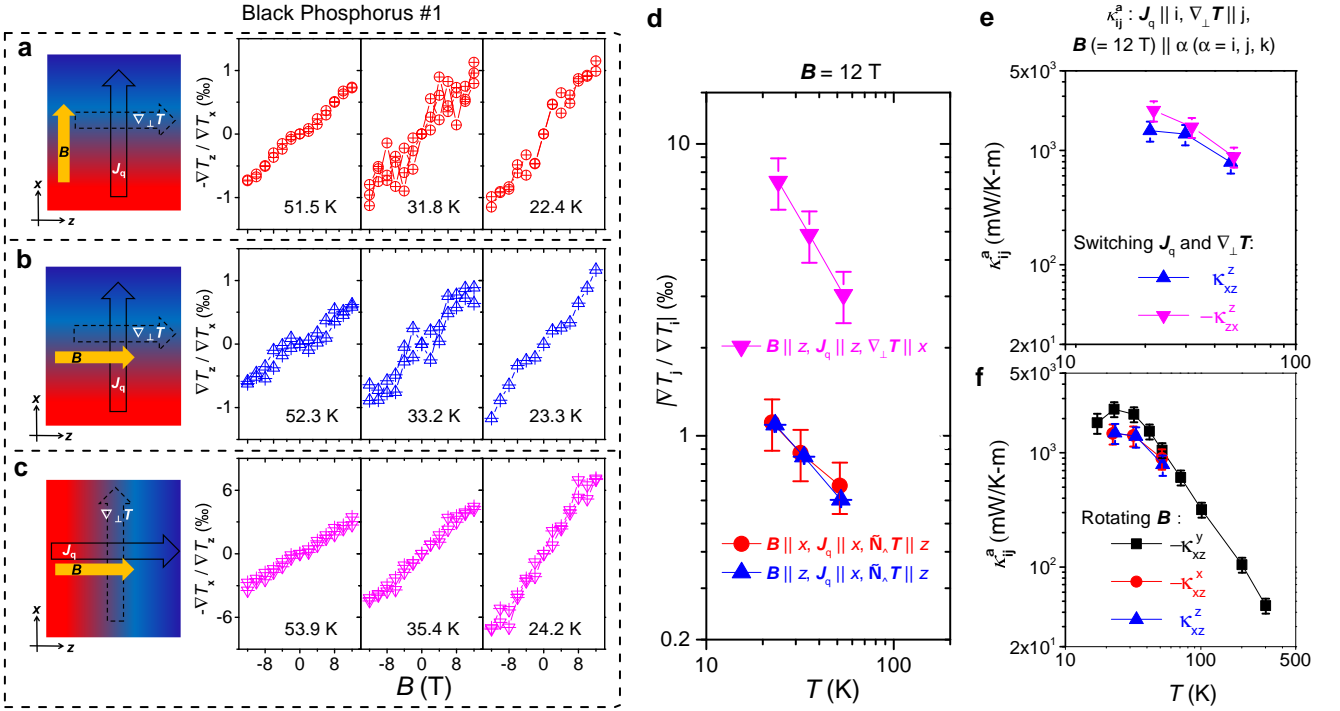


FIG. 2. **Planar thermal Hall data.** (a) The field dependence of thermal Hall angle $\nabla T_j / \nabla T_i$, with J_q and B along the x axis, $(\nabla T)_\perp$ along the z axis, at three typical temperatures. This allows to quantify κ_{xz}^x . (b) Same for J_q along the x axis, B and $(\nabla T)_\perp$ along the z axis. This allows to quantify κ_{xz}^z . (c) Same for J_q and B along the z axis and $(\nabla T)_\perp$ along the x axis. This allows to quantify κ_{zx}^z . (d) The temperature dependence of the thermal Hall angle for three different configurations at 12 T. All measurements are performed on the same sample. Note that the thermal Hall angle, $\nabla T_j / \nabla T_i$ is almost unchanged when the orientations of B rotates from J_q to $(\nabla T)_\perp$. On the other hand, it changes by a factor of six times when the orientations of J_q and $(\nabla T)_\perp$ permute with each other. This difference combined with the anisotropy in longitudinal thermal conductivity warrants Onsager reciprocity: $\kappa_{xz}^z = -\kappa_{zx}^z$, as seen in (e). (f) Comparison of thermal Hall conductivity κ_{xz} with the magnetic field B rotating from the orthogonal (y axis, from previous work [12] with the same sample) to the parallel direction of the J_q (x axis) or the $(\nabla T)_\perp$ (z axis).

In anisotropic dense medium, thermal diffusivity is a tensor, \bar{D} . The heat equation becomes :

$$\frac{\partial T}{\partial t} = \vec{\nabla} \cdot (\bar{D} \vec{\nabla} T) \quad (1)$$

Consider now the energy continuity equation, which relates the energy flux to specific heat per volume, C :

$$\vec{\nabla} \cdot \vec{J}_q + C \frac{\partial T}{\partial t} = 0 \quad (2)$$

The combination of the two previous equations leads to :

$$\vec{J}_q = -C \bar{D} \vec{\nabla} T \quad (3)$$

The thermal conductivity tensor $\bar{\kappa}$, is thus the thermal diffusivity tensor multiplied by a scalar: $\bar{\kappa} = \bar{D} C$. Therefore, off-diagonal components in $\bar{\kappa}$ are proportional to their counterparts in \bar{D} . The latter is the product of carrier velocity and carrier mean free path. Sound velocity, v_s , and phonon mean free path ℓ_{ph} (see Fig. 1c) are

both anisotropic at zero magnetic field. The issue is to find a way for magnetic field to skew one or both of these tensors off the symmetry axes

Recent theoretical studies have scrutinized intrinsic phonon band[31] incorporated with energy magnetization contribution [21, 32] and phonon angular momentum acquired through interaction with the spins [33, 34] or with orbital motion of ions [35].

Absent magnetism, the interplay between electric polarization and phonons deserves scrutiny. The computed map of charge distribution is strongly orientational [36]. Dipole-active phonon modes has been detected by infrared spectroscopy [37]. These are optical phonons and not heat-carrying acoustic modes which interest us. Nevertheless, any phonon breaking the inversion symmetry will generate an electric dipolar wave. This is a feature highlight in the context of ferrons, the elementary excitation of a ferroelectric solid, even in a paraelectric insulators [38, 39].

The thermal expansion of black P is not only anisotropic, but has opposite signs along armchair and

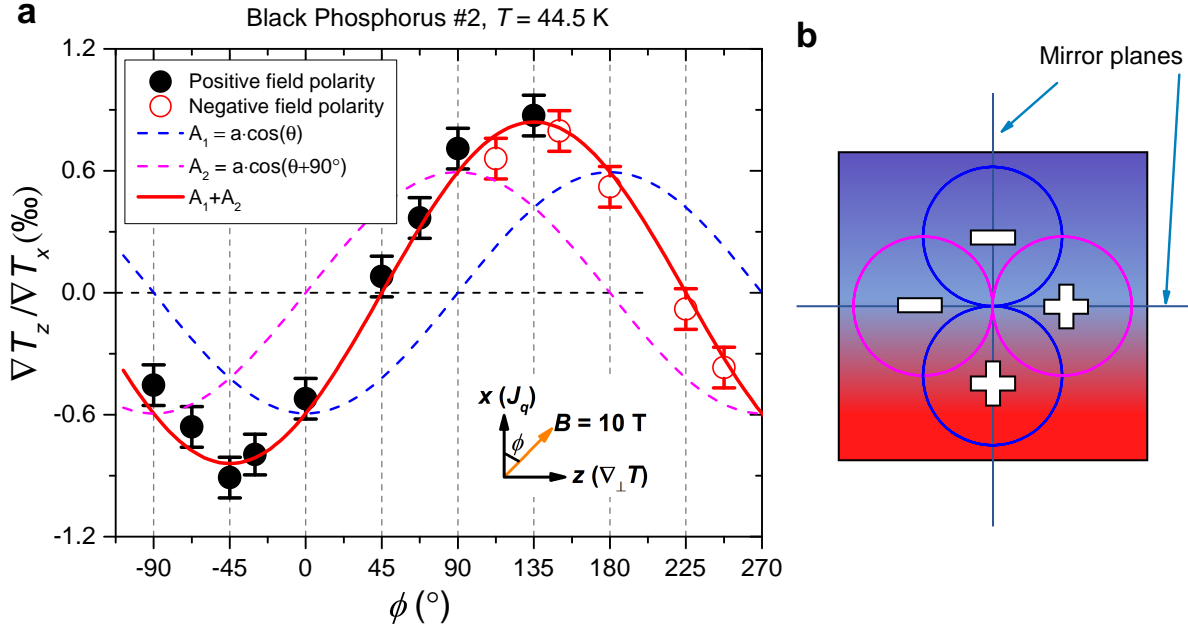


FIG. 3. **Angle dependence of the thermal Hall angle in the planar configuration.** (a) Angular dependence of $\nabla T_z / \nabla T_x$ at a constant temperature and constant magnetic field. The red line is a cosine fit to the data, and the sum of two blue lines representing $\cos\phi$ and $\cos(\phi + \pi/2)$. Each of these components peaks along one of the two high-symmetry axis and vanishes along the other symmetry axis. Suggesting that the planar thermal Hall signal consists of two distinct contributions each along one high-symmetry axis (b).

zigzag crystalline orientations [40]. As a consequence, in presence of a temperature gradient each tetragonal unit cell is slightly distorted. Its lattice parameter, compared to its colder or warmer neighboring cells, is longer and shorter along opposite (Fig. 4a) orientations. This paves the way for finite dipolar polarization, and for chirality in presence of the magnetic field. The inversion center of the pristine unit cell is not an atomic site and atomic displacements associated with phonons generate electric dipole moments (Fig. 4b). Therefore, acoustic phonons breaking inversion centers are traveling electric dipolar moments capable of coupling to a static magnetic field (Fig. 4c).

The torque exerted by a static magnetic field, \vec{B} , on an electric dipole of \vec{P} moving with a velocity of \vec{v} is: $\vec{\tau} = \vec{P} \times (\vec{B} \times \vec{v})$ [41]. Let us rewrite it as:

$$\vec{\tau} = (\vec{P} \cdot \vec{v}) \vec{B} - (\vec{P} \cdot \vec{B}) \vec{v} \quad (4)$$

Thus, the torque due to the Lorentz force exerted on each of the two poles is finite when the magnetic field is oriented perpendicular to the orientation of the dipole propagation (Fig. 4d). These are ingredients for a scenario for planar thermal Hall signal in a non-magnetic insulator (see the supplement [30] for a discussion of the expected angular variation). A rigorous treatment is beyond the scope of this paper. However, let us compare the order of magnitude of the expected and the measured signals.

Experimentally, the thermal Hall angle at $B = 10$ T peaks to $\approx \times 10^{-2}$ in black P. The length scale extracted from this angle and fundamental constants ($\lambda_{tha} = \ell_B \sqrt{\kappa_{ij}/\kappa_{jj}}$) is about 5 Å. Intriguingly, in all insulators displaying a thermal Hall signal, this length scale lies in a narrow range ($2 \text{ \AA} < \lambda_{tha} < 7 \text{ \AA}$ [12, 14]. As seen in figure S2 in the supplement [30], this remains true for recently studied cases of Si, Ge and quartz [15].

Suppose an electric dipole moment of δp traveling with the velocity of sound, v_s (loosely linked to the Debye frequency by $v_s \sim a\omega_D$, where a is the interatomic distance). The exerted torque, that is the angular derivative of the energy, would be $B a \omega_D \delta p$. Divided by the Debye energy, it yields $\theta_H \simeq \frac{a \delta p}{\hbar} B$, the order of magnitude of the expected rotation angle. With $\ell_B^2 = \frac{\hbar}{eB}$, assuming $\delta p \approx ea$, leads to:

$$\theta_H \approx \frac{a^2}{\ell_B^2} \quad (5)$$

This expectation is of the order of magnitude of the measured signal. A rigorous treatment would presumably include in this expression the Grüneisen parameter [42]. Possibly, the atomic electric dipole polarizability [43] would also be present. However, the former, which is dimensionless remains of the order of unity and the latter introduces a length scale which does not vary widely among different solids. Therefore, a scenario attribut-

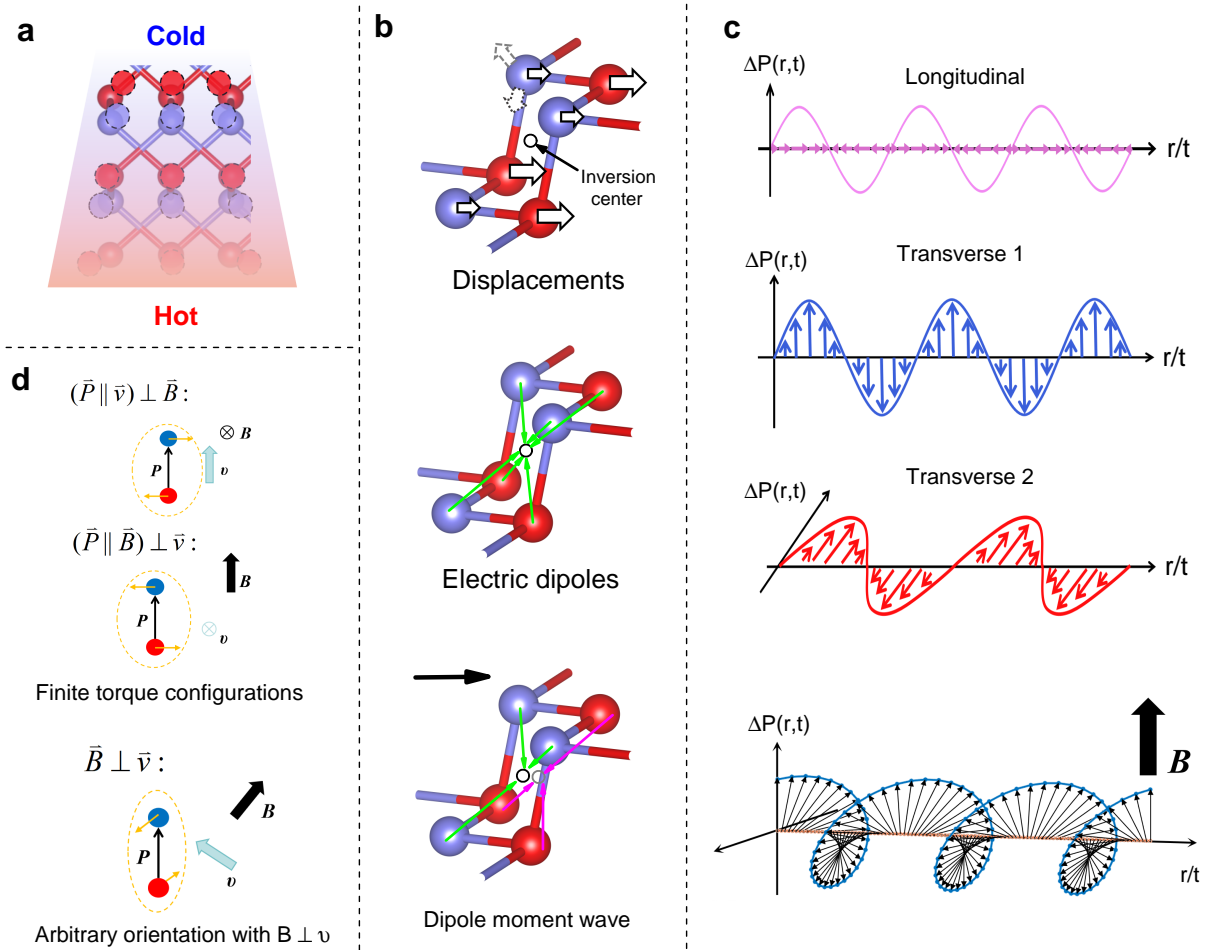


FIG. 4. **From atomic displacements to dipolar moments** (a) Lattice distortion due to the thermal expansion. (b) Phosphorus atoms surrounding an inversion center. Their displacements associated with an acoustic mode (top) will affect the local electric dipole moments (middle), generating a net dipole moment (bottom). (c) Phonon modes are associated with waves of dipolar moments. A static magnetic field will exert a torque on the dipole moment traveling with the sound wave. (d) This torque ($\tau = \vec{P} \times (\vec{B} \times \vec{v})$) will survive only when the magnetic field is oriented perpendicular to the wave velocity. Orange arrows show the orientation of the Lorentz forces on the two poles of the dipole.

ing the thermal Hall signal to the interaction between a static magnetic field and traveling electric dipolar waves emerges promising from our study.

We thank Benoît Fauqué for stimulating discussions. This work was supported by the National Key Research and Development Program of China (Grant No. 2022YFA1403500), the National Science Foundation of China (Grant No. 12004123, 51861135104 and 11574097), and the Fundamental Research Funds for the Central Universities (Grant no. 2019kfyXMBZ071). X. L. was supported by The National Key Research and Development Program of China (Grant No.2023YFA1609600) and the National Science Foundation of China (Grant No. 12304065).

* lixiaokang@hust.edu.cn
† zengwei.zhu@hust.edu.cn
‡ kamran.behnia@espci.fr

- [1] C. Strohm, G. L. J. A. Rikken, and P. Wyder, Phenomenological evidence for the phonon Hall effect, *Phys. Rev. Lett.* **95**, 155901 (2005).
- [2] K. Sugii, M. Shimozawa, D. Watanabe, Y. Suzuki, M. Halim, M. Kimata, Y. Matsumoto, S. Nakatsuji, and M. Yamashita, Thermal Hall effect in a phonon-glass $\text{Ba}_3\text{CuSb}_2\text{O}_9$, *Phys. Rev. Lett.* **118**, 145902 (2017).
- [3] X. Li, B. Fauqué, Z. Zhu, and K. Behnia, Phonon thermal Hall effect in strontium titanate, *Phys. Rev. Lett.* **124**, 105901 (2020).
- [4] G. Grissonnanche, S. Thériault, A. Gourgout, M.-E. Boulanger, E. Lefrançois, A. Ataei, F. Laliberté, M. Dion, J.-S. Zhou, S. Pyon, *et al.*, Chiral phonons in the pseudo-

- gap phase of cuprates, *Nature Physics* **16**, 1108 (2020).
- [5] M.-E. Boulanger, G. Grissonnanche, S. Badoux, A. Lalire, É. Lefrançois, A. Legros, A. Gourgout, M. Dion, C. Wang, X. Chen, *et al.*, Thermal Hall conductivity in the cuprate mott insulators Nd_2CuO_4 and $\text{Sr}_2\text{CuO}_2\text{Cl}_2$, *Nature Communications* **11**, 1 (2020).
- [6] M. Akazawa, M. Shimozawa, S. Kittaka, T. Sakakibara, R. Okuma, Z. Hiroi, H.-Y. Lee, N. Kawashima, J. H. Han, and M. Yamashita, Thermal Hall effects of spins and phonons in kagome antiferromagnet Cd-Kapellasite, *Phys. Rev. X* **10**, 041059 (2020).
- [7] S. Sim, H. Yang, H.-L. Kim, M. J. Coak, M. Itoh, Y. Noda, and J.-G. Park, Sizable suppression of thermal Hall effect upon isotopic substitution in SrTiO_3 , *Phys. Rev. Lett.* **126**, 015901 (2021).
- [8] L. Chen, M.-E. Boulanger, Z.-C. Wang, F. Tafti, and L. Taillefer, Large phonon thermal Hall conductivity in the antiferromagnetic insulator Cu_3TeO_6 , *Proceedings of the National Academy of Sciences* **119**, e2208016119 (2022).
- [9] T. Uehara, T. Ohtsuki, M. Udagawa, S. Nakatsuji, and Y. Machida, Phonon thermal Hall effect in a metallic spin ice, *Nature Communications* **13**, 1 (2022).
- [10] S. Jiang, X. Li, B. Fauqué, and K. Behnia, Phonon drag thermal Hall effect in metallic strontium titanate, *Proceedings of the National Academy of Sciences* **119**, e2201975119 (2022).
- [11] E. Lefrançois, G. Grissonnanche, J. Baglo, P. Lampen-Kelley, J.-Q. Yan, C. Balz, D. Mandrus, S. E. Nagler, S. Kim, Y.-J. Kim, N. Doiron-Leyraud, and L. Taillefer, Evidence of a phonon Hall effect in the Kitaev spin liquid candidate $\alpha\text{-RuCl}_3$, *Phys. Rev. X* **12**, 021025 (2022).
- [12] X. Li, Y. Machida, A. Subedi, Z. Zhu, L. Li, and K. Behnia, The phonon thermal Hall angle in black phosphorus, *Nature Communications* **14**, 1027 (2023).
- [13] R. Sharma, M. Bagchi, Y. Wang, Y. Ando, and T. Lorenz, Phonon thermal Hall effect in charge-compensated topological insulators, *Phys. Rev. B* **109**, 104304 (2024).
- [14] Q. Meng, X. Li, L. Zhao, C. Dong, Z. Zhu, and K. Behnia, Thermal Hall effect driven by phonon-magnon hybridization in a honeycomb antiferromagnet (2024), [arXiv:2403.13306 \[cond-mat.str-el\]](https://arxiv.org/abs/2403.13306).
- [15] X. Jin, X. Zhang, W. Wan, H. Wang, Y. Jiao, and S. Li, Discovery of universal phonon thermal Hall effect in crystals, [arXiv preprint arXiv:2404.02863](https://arxiv.org/abs/2404.02863) (2024).
- [16] L. Chen, É. Lefrançois, A. Vallipuram, Q. Barthélemy, A. Ataie, W. Yao, Y. Li, and L. Taillefer, Planar thermal Hall effect from phonons in a kitaev candidate material, *Nature Communications* **15**, 3513 (2024).
- [17] Q. Barthélemy, Étienne Lefrançois, L. Chen, A. Vallipuram, K. M. Zoch, C. Krellner, P. Puphal, and L. Taillefer, Planar parallel phonon Hall effect and local symmetry breaking (2023), [arXiv:2310.19682 \[cond-mat.str-el\]](https://arxiv.org/abs/2310.19682).
- [18] L. Sheng, D. N. Sheng, and C. S. Ting, Theory of the phonon Hall effect in paramagnetic dielectrics, *Phys. Rev. Lett.* **96**, 155901 (2006).
- [19] Y. Kagan and L. A. Maksimov, Anomalous Hall effect for the phonon heat conductivity in paramagnetic dielectrics, *Phys. Rev. Lett.* **100**, 145902 (2008).
- [20] L. Zhang, J. Ren, J.-S. Wang, and B. Li, Topological nature of the phonon Hall effect, *Phys. Rev. Lett.* **105**, 225901 (2010).
- [21] T. Qin, J. Zhou, and J. Shi, Berry curvature and the phonon Hall effect, *Phys. Rev. B* **86**, 104305 (2012).
- [22] B. K. Agarwalla, L. Zhang, J.-S. Wang, and B. Li, Phonon Hall effect in ionic crystals in the presence of static magnetic field, *The European Physical Journal B* **81**, 197 (2011).
- [23] J.-Y. Chen, S. A. Kivelson, and X.-Q. Sun, Enhanced thermal Hall effect in nearly ferroelectric insulators, *Phys. Rev. Lett.* **124**, 167601 (2020).
- [24] B. Flebus and A. H. MacDonald, Charged defects and phonon Hall effects in ionic crystals, *Phys. Rev. B* **105**, L220301 (2022).
- [25] H. Guo, D. G. Joshi, and S. Sachdev, Resonant thermal Hall effect of phonons coupled to dynamical defects, *Proceedings of the National Academy of Sciences* **119**, e2215141119 (2022).
- [26] L. Mangeolle, L. Balents, and L. Savary, Phonon thermal Hall conductivity from scattering with collective fluctuations, *Phys. Rev. X* **12**, 041031 (2022).
- [27] Y. Machida, A. Subedi, K. Akiba, A. Miyake, M. Tokunaga, Y. Akahama, K. Izawa, and K. Behnia, Observation of poiseuille flow of phonons in black phosphorus, *Science Advances* **4**, eaat3374 (2018).
- [28] B. Sun, X. Gu, Q. Zeng, X. Huang, Y. Yan, Z. Liu, R. Yang, and Y. K. Koh, Temperature dependence of anisotropic thermal-conductivity tensor of bulk black phosphorus, *Advanced Materials* **29**, 1603297 (2017).
- [29] Y. Fujii, Y. Akahama, S. Endo, S. Narita, Y. Yamada, and G. Shirane, Inelastic neutron scattering study of acoustic phonons of black phosphorus, *Solid State Communications* **44**, 579 (1982).
- [30] See Supplemental Material for more details (2024).
- [31] Y.-F. Yang, G.-M. Zhang, and F.-C. Zhang, Universal behavior of the thermal Hall conductivity, *Phys. Rev. Lett.* **124**, 186602 (2020).
- [32] T. Qin, Q. Niu, and J. Shi, Energy magnetization and the thermal hall effect, *Phys. Rev. Lett.* **107**, 236601 (2011).
- [33] L. Zhang and Q. Niu, Angular momentum of phonons and the Einstein–de Haas effect, *Phys. Rev. Lett.* **112**, 085503 (2014).
- [34] L. Zhang and Q. Niu, Chiral phonons at high-symmetry points in monolayer hexagonal lattices, *Phys. Rev. Lett.* **115**, 115502 (2015).
- [35] D. M. Juraschek and N. A. Spaldin, Orbital magnetic moments of phonons, *Phys. Rev. Mater.* **3**, 064405 (2019).
- [36] Z.-X. Hu, X. Kong, J. Qiao, B. Normand, and W. Ji, Interlayer electronic hybridization leads to exceptional thickness-dependent vibrational properties in few-layer black phosphorus, *Nanoscale* **8**, 2740 (2016).
- [37] S. Sugai and I. Shirovani, Raman and infrared reflection spectroscopy in black phosphorus, *Solid State Communications* **53**, 753 (1985).
- [38] B. L. Wooten, R. Iguchi, P. Tang, J. S. Kang, K. Uchida, G. E. W. Bauer, and J. P. Heremans, Electric field-dependent phonon spectrum and heat conduction in ferroelectrics, *Science Advances* **9**, eadd7194 (2023).
- [39] G. Bauer, P. Tang, R. Iguchi, J. Xiao, K. Shen, Z. Zhong, T. Yu, S. Rezende, J. Heremans, and K. Uchida, Polarization transport in ferroelectrics, *Phys. Rev. Appl.* **20**, 050501 (2023).
- [40] H. Sun, G. Liu, Q. Li, and X. Wan, First-principles study of thermal expansion and thermomechanics of single-layer black and blue phosphorus, *Physics Letters A* **380**, 2098 (2016).

- [41] C. E. Mungan and A. Lasinski, Motion of an electric dipole in a static electromagnetic field, *Latin-American Journal of Physics Education* **2**, 192 (2008).
- [42] N. W. Ashcroft and N. D. Mermin, *Solid State Physics* (Holt-Saunders, 1976).
- [43] P. Schwerdtfeger and J. K. Nagle, 2018 table of static dipole polarizabilities of the neutral elements in the periodic table*, *Molecular Physics* **117**, 1200 (2019).

Supplementary Materials for “Angle-dependent planar thermal Hall effect in black phosphorus”

Materials and Methods

Black phosphorus crystals used in this work are same to our previous report [34]. They were synthesized under high pressure and came from two different sources. Sample #1 was obtained commercially and sample #2 was kindly provided by Prof. Yuichi Akahama (University of Hyogo).

All thermal transport experiments were performed in a commercial measurement system (Quantum Design PPMS) within a stable high-vacuum sample chamber. An one-heater-four-thermocouples (type E) techniques was employed to simultaneously measure the longitudinal and transverse thermal gradient. The thermal gradient in the sample was produced through a 4.7 kΩ chip resistor alimented by a current source (Keithley6221). The DC voltage on the heater and thermocouples (thermometers) was measured through the DC-nanovoltmeter (Keithley2182A). The thermocouples, the heat-sink, and the heater were connected to samples directly or by gold wires with a 50 microns diameter. All contacts on the sample were made using silver paste. In the angular dependent measurements, a thermal transport rotation probe was used.

The longitudinal (∇T_i) and the transverse (∇T_j) thermal gradient generated by a longitudinal thermal current J_q were measured. They lead to the longitudinal (κ_{ii}) and the transverse (κ_{ij}) thermal conductivity, as well as the thermal Hall angle ($\nabla T_j/\nabla T_i$):

$$\kappa_{ii} = \frac{Q_i}{\nabla T_i} \quad (\text{S1})$$

$$\frac{\nabla T_j}{\nabla T_i} = \frac{\kappa_{ij}}{\kappa_{jj}} \quad (\text{S2})$$

$$\kappa_{ij} = \frac{\nabla T_j}{\nabla T_i} \cdot \kappa_{jj} \quad (\text{S3})$$

Here Q is the heat power.

Raw data of angular dependent planar thermal Hall effect

Fig. S1 shows the field dependent thermal Hall angles ($\nabla T_j/\nabla T_i$) with the J_q alongs x axis and the $(\nabla T)_\perp$ along z axis at six different field orientations. ϕ is the angle of the magnetic field with respect to the J_q (x axis). $\phi = 0^\circ$ and $\phi = 90^\circ$ represent the orientations along two high-symmetry axes, and their $\nabla T_j/\nabla T_i$ signal

have the same amplitude but opposite signs. $\phi = -45^\circ$ and $\phi = 45^\circ$ represent two diagonal orientations of the puckered honeycomb plane that have the maximum and vanished responses respectively, suggesting that the planar thermal Hall signal consists of two distinct contributions each along one high-symmetry axis. $\phi = -45^\circ$ and $\phi = 135^\circ$ have signals with opposite signs, as expected from the antisymmetric operation ($\kappa_{ij}(\mathbf{B}) = -\kappa_{ij}(-\mathbf{B})$).

Torque exerted by the magnetic field on moving dipoles

The torque exerted by a static magnetic field, \vec{B} , on an electric dipole of \vec{P} moving with a velocity of \vec{v} is :

$$\begin{aligned} \vec{\tau} &= \vec{P} \times (\vec{B} \times \vec{v}) \\ &= (\vec{v} \times \vec{B}) \times \vec{P} \\ &= (\vec{P} \cdot \vec{v})\vec{B} - (\vec{P} \cdot \vec{B})\vec{v} \end{aligned} \quad (\text{S4})$$

The electric dipole \vec{P} , field \vec{B} , and the velocity \vec{v} can be expanded as:

$$\begin{aligned} \vec{P} &= P_x \vec{e}_x + P_y \vec{e}_y + P_z \vec{e}_z; \\ \vec{B} &= B_x \vec{e}_x + B_y \vec{e}_y + B_z \vec{e}_z; \\ \vec{v} &= v_x \vec{e}_x + v_y \vec{e}_y + v_z \vec{e}_z. \end{aligned} \quad (\text{S5})$$

Thus, the S4 can be rewritten as:

$$\begin{aligned} \vec{\tau} &= (P_x v_x + P_y v_y + P_z v_z) \cdot (B_x \vec{e}_x + B_y \vec{e}_y + B_z \vec{e}_z) \\ &\quad - (P_x B_x + P_y B_y + P_z B_z) \cdot (v_x \vec{e}_x + v_y \vec{e}_y + v_z \vec{e}_z) \\ &= (P_y v_x B_x + P_z v_z B_x - P_y B_y v_x - P_z B_z v_x) \cdot \vec{e}_x \\ &\quad + (P_x v_y B_y + P_z v_z B_y - P_x B_x v_y - P_z B_z v_y) \cdot \vec{e}_y \\ &\quad + (P_x v_x B_z + P_y v_y B_z - P_x B_x v_z - P_y B_y v_z) \cdot \vec{e}_z \end{aligned} \quad (\text{S6})$$

The angular dependence of the torque and the observed bi-axial symmetry

In our experiment, the magnetic field was rotated in the xz plane, the longitudinal thermal gradient thermal gradient was applied along the x -axis. Putting $B_y = 0$ and $P_y = 0$, Equation S6 becomes:

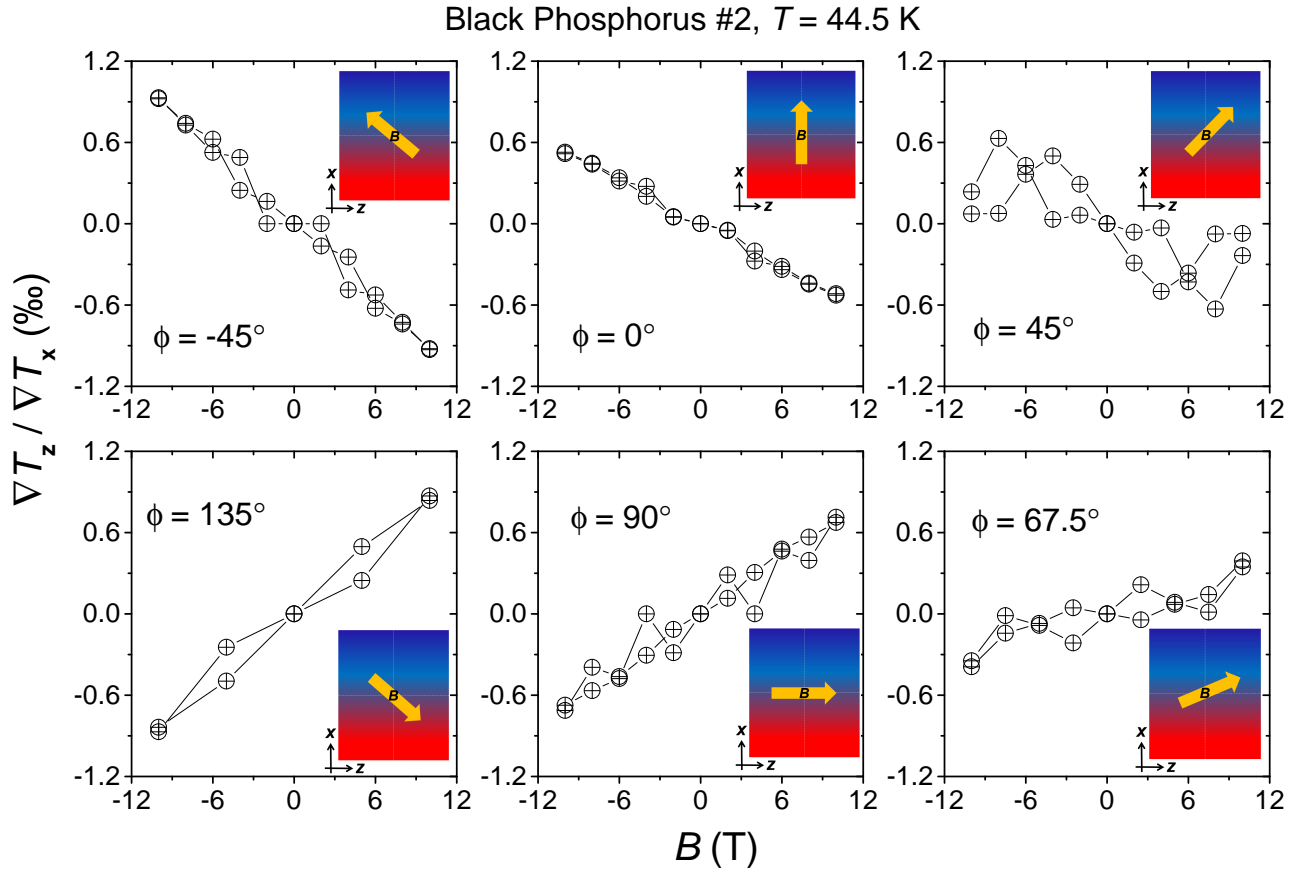


FIG. S1. **Raw data of angular dependent planar thermal Hall effect in Black phosphorus.** Field dependent thermal Hall angle ($\nabla T_z / \nabla T_x$) at a constant temperature and six different field orientations.

$$\begin{aligned}
 \vec{\tau} = & (P_z v_z B_x - P_z B_z v_x) \cdot \vec{e}_x \\
 & - (P_x B_x v_y + P_z B_z v_y) \cdot \vec{e}_y \\
 & + (P_x v_x B_z - P_x B_x v_z) \cdot \vec{e}_z
 \end{aligned} \quad (S7)$$

We measured the transverse thermal gradient along the

z -axis. The torque along the z -axis is equal to :

$$\tau_z = (P_x v_x) B_z - (P_x v_z) B_x \quad (S8)$$

One can see that the expected torque along the z -axis has two components. Each of them vanishes when the field is along either the x -axis or the z -axis. This is in agreement with the experimental data seen in Fig. 3 of the main text.

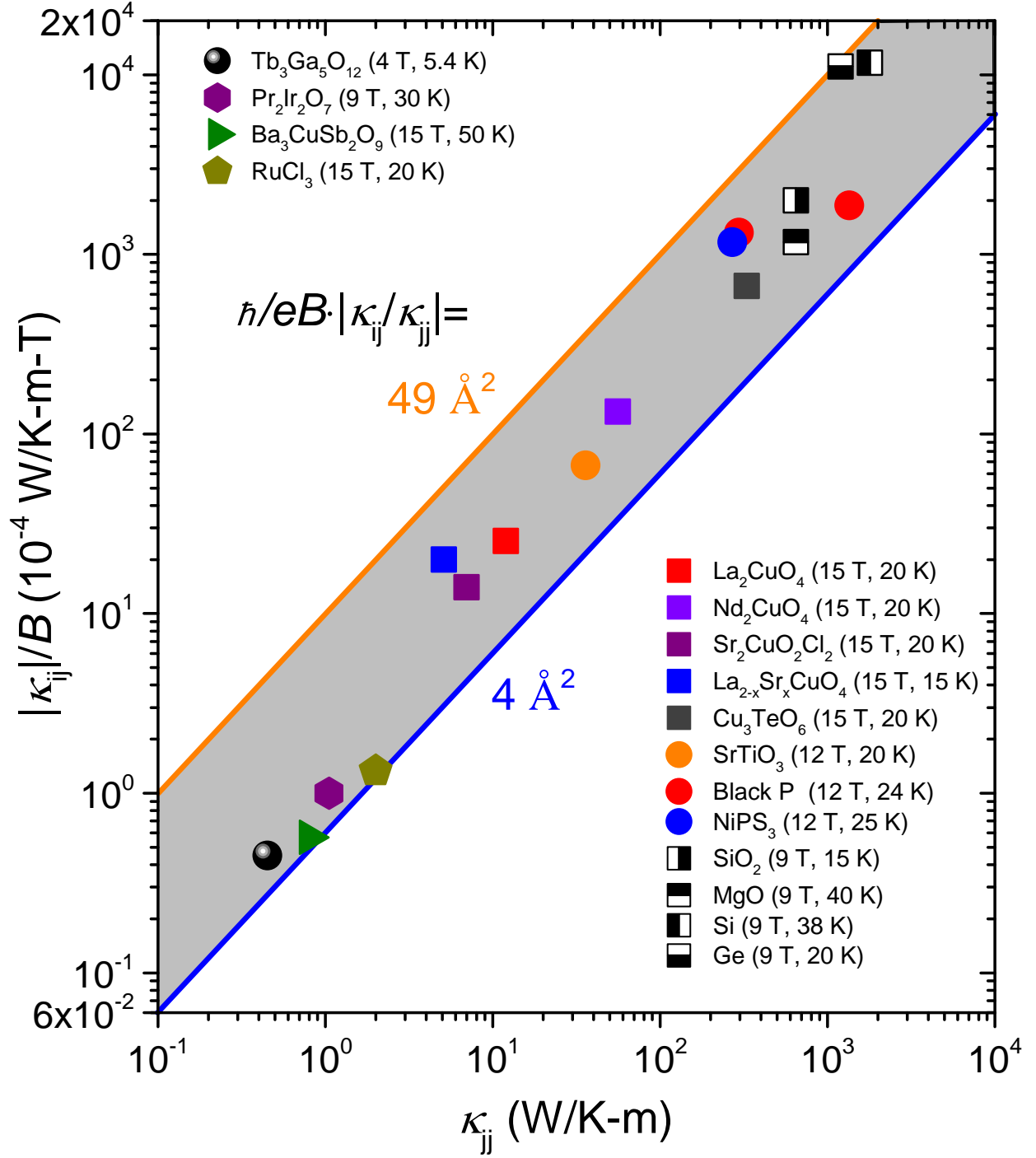


FIG. S2. **Thermal Hall angle in different insulators** The transverse thermal conductivity divided by magnetic field as a function of longitudinal thermal conductivity in different insulators (source: [1–6, 8, 9, 11, 12, 14, 15]).